ACS APPLIED MATERIALS & INTERFACES

Research Article

www.acsami.org

Oxidation Behavior of Multiwalled Carbon Nanotubes Fluidized with Ozone

Danny C. Vennerberg,[†] Rafael L. Quirino,[†] Youngchan Jang,[‡] and Michael R. Kessler*[,†,§]

[†]Department of Materials Science and Engineering, Iowa State University, Ames, Iowa 50011, United States

[‡]Kumho Petrochemical R&BD Center, Daejeon 305-600, South Korea

[§]School of Mechanical and Materials Engineering, Washington State University, Pullman, Washington 99164, United States

ABSTRACT: Multiwalled carbon nanotubes (MWCNTs) were simultaneously fluidized and oxidized with gaseous ozone in a vertical reactor. Two different varieties of MWCNTs were compared to determine the versatility of the treatment and to elucidate the effect of defects on the oxidation behavior of MWCNTs. The extent of oxidation and nature of functional groups introduced on the nanotube surfaces were determined using Fourier-transform infrared spectroscopy (FTIR), X-ray photoelectron spectroscopy (XPS), and Boehm titration, and structural changes were monitored with Raman spectroscopy, scanning electron microscopy (SEM), and transmission electron microscopy (TEM). After only a few minutes of treatment, nongraphitic impurities were removed from the MWCNTs, and significant levels of oxidation (~8 atom % O) were achieved with very little damage to the nanotube sidewalls. Short O_3 exposure resulted in primarily hydroxyl functionalities, whereas longer exposure led to the formation of mainly carboxylic acid groups. Aliphatic defects present in the commercially produced MWCNTs were found to play an important role in the oxidation mechanism. Because of its ability to remove impurities and to evenly oxidize the sidewalls of nanotubes without the use of any solvents, the fluidized O_3 reaction developed in this study was found to be an attractive option for industrial-scale MWCNT functionalization.

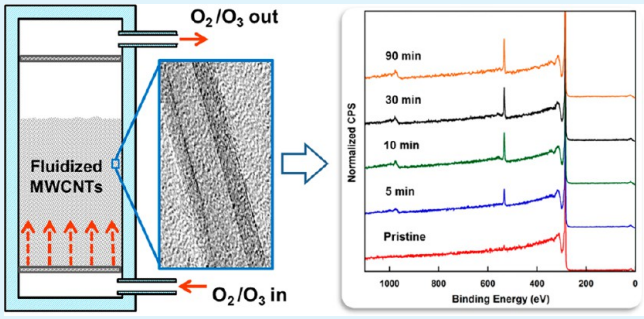

KEYWORDS: *multiwalled carbon nanotube, oxidation, functionalization, fluidized bed, ozone, surface treatment*

1. INTRODUCTION

Carbon nanotubes (CNTs) possess extraordinary mechanical, thermal, and electrical properties, making them ideal candidates for a wide range of applications in areas as diverse as energy storage,[1,2] electronics,[3] and biosensors.[4,5] CNTs are expected to be particularly suitable as reinforcement for composites because of their high aspect ratio. However, the addition of CNTs to polymers does not always engender outstanding mechanical properties and, in fact, has been reported to have deleterious effects in some instances.[6,7] This underperformance stems from several possible sources. The graphene walls of as-grown CNTs are hydrophobic and have low surface energy, making CNTs incompatible with polar solvents and most polymer matrix materials. Furthermore, strong intertube van der Waals attractions cause CNTs to agglomerate into bundles, which have poor mechanical properties. Surface modification is an established approach to overcome poor dispersion and weak interfacial bonding in CNT-reinforced composites. Oxidation of CNTs by exposure to concentrated acids is a popular functionalization method on the laboratory-scale that has proven to be effective in improving composite properties.[8−12] However, acid exposure causes significant damage to the nanotube structure and leaves behind weakly adsorbed debris, which interferes with interfacial bonding in a composite if it is not removed.[13] Acid oxidation is also unattractive for industrial-scale functionalization because of safety hazards associated with flammable and corrosive acids as well as the need to repeatedly wash and dry the CNTs postreaction. Furthermore, any functionalization methods involving the use of solvents generates liquid waste containing CNTs. Proper disposal of such waste provides a costly challenge and may be subject to regulatory scrutiny for environmental and health reasons.

Alternative, gas-phase oxidation reactions eliminate waste and drying steps, making them appealing for mass production of functionalized CNTs. Oxidation by gaseous O_3 is particularly well-suited for industrial use because O_3 is currently generated inexpensively in large quantities and readily decomposes to O_2 in water or upon reaction with unsaturated molecules.[14] Several reports of successful functionalization of single-walled carbon nanotubes (SWCNTs) using O_3 have been reported in the literature beginning with Smalley et al.[15−19] As with other fullerenes, the curvature strain of small diameter SWCNTs makes them reactive towards O_3, and a variety of oxygen-bearing functional groups can be generated including alcohols, ketones, esters, and carboxylic acids. These moieties permit the SWCNTs to disperse much more easily in solvents. For

Received: October 30, 2013
Accepted: January 14, 2014
Published: January 14, 2014

   dx.doi.org/10.1021/am4048305 | ACS Appl. Mater. Interfaces 2014, 6, 1835−1842

instance, SWCNTs simultaneously exposed to UV light and O_3 were functionalized with hydroxyl and carbonyl groups, which increased their solubility in ethanol by more than 500%.[16] Multiwalled carbon nanotubes (MWCNTs) are also reactive towards O_3, although less so than SWCNTs because of their larger diameters. A few reports have shown that by sonicating MWCNTs in water and bubbling O_3 through the dispersion oxidation levels on the order of 3−7% can be achieved.[20−22] Functionalization of MWCNTs by gaseous O_3 has not been as well studied as SWCNTs, but a few reports indicate that significant oxidation is possible.[23−25] Kim et al. used a single UV−O_3 source to endow MWCNTs with approximately 5 atom % oxygen after 1 h of exposure.[23] Zhang et al. used an O_3/water vapor mixture to generate oxygenated functional groups, although substantial damage to the tube walls was observed upon prolonged exposure.[25]

Although gas-phase O_3 reactions have been shown to oxidize both SWCNTs and MWCNTs successfully, achieving uniform oxidation of nanotubes within a macroscopic agglomeration remains a challenge,[19] especially as the reaction size scales up. Thus, previously reported methods are not suitable for large-scale functionalization. High-quality MWCNTs are currently available in huge quantities at low cost, and market forecasts predict further increases in production to 12 800 metric tons by 2016 with concomitant price declines.[26] With a scalable, inexpensive functionalization method, widespread use of MWCNT-reinforced composites is a realistic possibility in the near future.

This work is part of a program to develop industrially scalable functionalization methods for MWCNTs that do not require solvents or acids and that do not significantly damage the nanotube structure. Here, we discuss our efforts to purify rapidly and evenly and to functionalize MWCNTs using an O_3/O_2 mixture as the bubbling gas in a fluidized bed reactor. In contrast to previous reports on the oxidation of MWCNTs with gaseous O_3, the fluidized bed employed in this method allows for uniform treatment of large quantities of CNTs. A corona-discharge O_3 source, the most cost-effective method of producing O_3 on a large scale, is used instead of the UV−O_3 type generators popular in past work. Two types of commercially available MWCNTs with similar size but different defect densities were treated to elucidate differences in oxidation behavior and to determine the versatility of the method. Structural changes in the nanotubes were monitored by transmission electron microscopy (TEM), scanning electron microscopy (SEM), and Raman spectroscopy, and oxidation was characterized with Fourier-transform infrared spectroscopy (FTIR), X-ray photoelectron spectroscopy (XPS), and Boehm titration.

2. EXPERIMENTAL DETAILS

2.1. Materials. Kumho multiwalled carbon nanotubes (*k*-MWCNTs) with an average diameter of 10 nm and purity greater than 90% were supplied by Kumho Petrochemical Co. (South Korea). NC7000 multiwalled carbon nanotubes (*n*-MWCNTs) with an average diameter of 10 nm and purity of 90% were supplied by Nanocyl, S.A. (Belgium). O_3 was produced with a corona-discharge O_3 generator (L-50, Ozonology Inc.) using O_2 as the feed gas.

2.2. Fluidized Ozone Treatment. Pristine MWCNTs (1 g) were placed into an empty gas purifier flask that was adapted for use as a fluidized bed, as shown schematically in Figure 1. An O_3/O_2 mixture containing 6% (w/w) O_3 was then flushed through the glassware from the lower insertion at a flow rate of 1.4 L/min through a stainless steel distributor plate, causing the MWCNTs to fluidize. A porous membrane affixed to the top of the reactor allowed venting of excess gas, which was scrubbed into a 2% potassium iodide solution to remove any remaining O_3 before discharging to atmosphere in a fume hood. The MWCNTs were treated for 5−90 min at a relative humidity of about 50%.

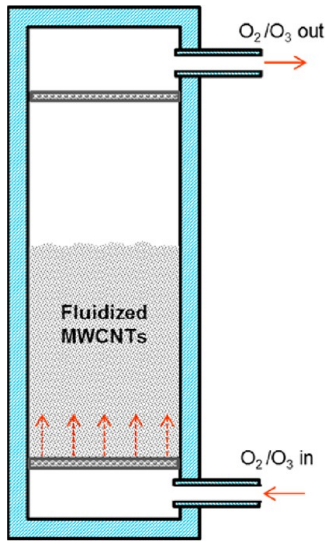

Figure 1. Schematic depiction of fluidized bed reactor.

2.3. Characterization. The structures of pristine and oxidized MWCNTs were probed with TEM (JEOL 1200EX), SEM (FEI Quanta 200), and Raman spectroscopy. Raman spectra were collected with a Renishaw inVia spectrometer using back-scattered light from a 488 nm laser focused through a 50× objective lens. Changes in surface chemistry were monitored with XPS, Boehm titration, and FTIR. FTIR spectra were collected in a Bruker IFS66 V spectrometer. The nanotubes were thoroughly mixed with potassium bromide and pressed into a pellet before data acquisition. XPS measurements were carried out in a Physical Electronics 5500 Multitechnique system with a monochromatic Al Kα radiation source, and CasaXPS software was employed for data processing. Analysis of the elemental surface composition of each sample was performed using MWCNTs taken from at least five different regions of the fluidized bed. An optimized acid−base (Boehm) titration technique was used to determine the concentration of protic functional groups on the surface of MWCNTs.[27] Briefly, MWCNTs were stirred overnight in three different 0.05 M basic solutions of NaOH, Na_2CO_3, and $NaHCO_3$. The samples were then filtered to remove the MWCNTs, and 10 mL aliquots of the filtrate were saved for analysis. Twenty milliliters of 0.05 M HCl was then added to the NaOH and the $NaHCO_3$ filtrate aliquots, and 30 mL of 0.05 M HCl was added to the Na_2CO_3 filtrate aliquot. Once the aliquots were acidified, they were back-titrated with 0.05 M NaOH, and the end point was determined with a digital pH meter. Triplicate titrations were performed for each sample.

3. RESULTS AND DISCUSSION

3.1. Material Assessment. As-produced MWCNTs may contain a variety of structural defects and impurities that critically affect their reactivity and ultimate performance. Amorphous carbon adsorbed to the surface of a MWCNT is chemically less stable than the nanotube sidewall and therefore will react preferentially with reagents intended to modify the MWCNT. Removal of amorphous carbon is necessary for covalent bonds to be formed directly with the MWCNT sidewall.[13] This study compares the oxidation behavior of two types of commercially available MWCNTs that are both produced by chemical vapor deposition (CVD) and have the same nominal dimensions and carbon purity levels. However, although SEM (Figures 2a and 3a) imaging shows no

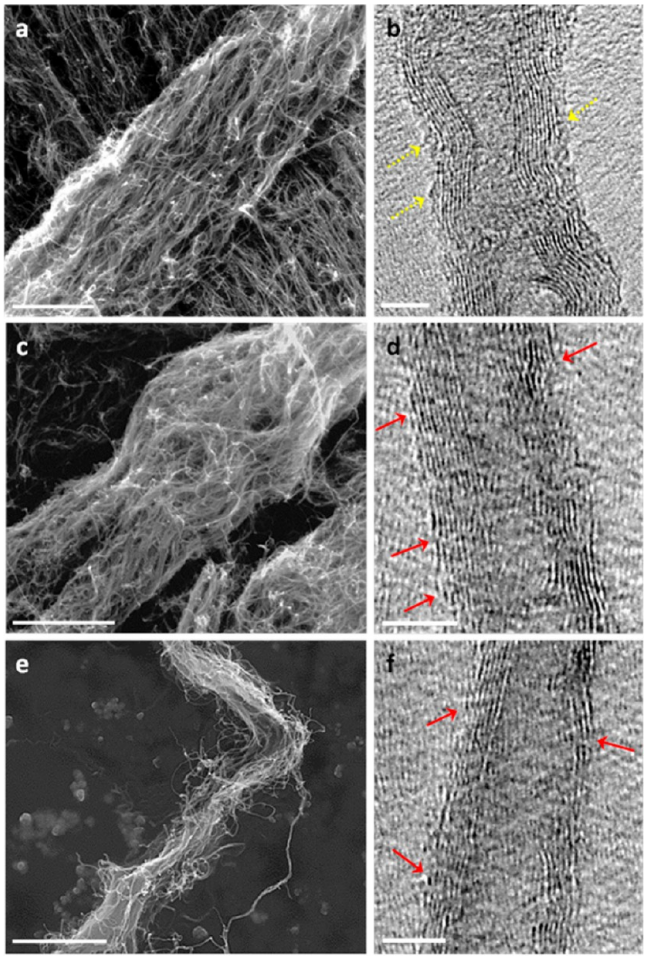

Figure 2. Representative SEM and TEM images of pristine *n*-MWCNTs (a, b) as-received, (c, d) fluidized for 10 min, and (e, f) fluidized for 90 min. Scale bars represent 1 μm and 5 nm for SEM and TEM images, respectively. Red arrows demarcate sidewall functionalization, and dashed yellow arrows highlight amorphous carbon.

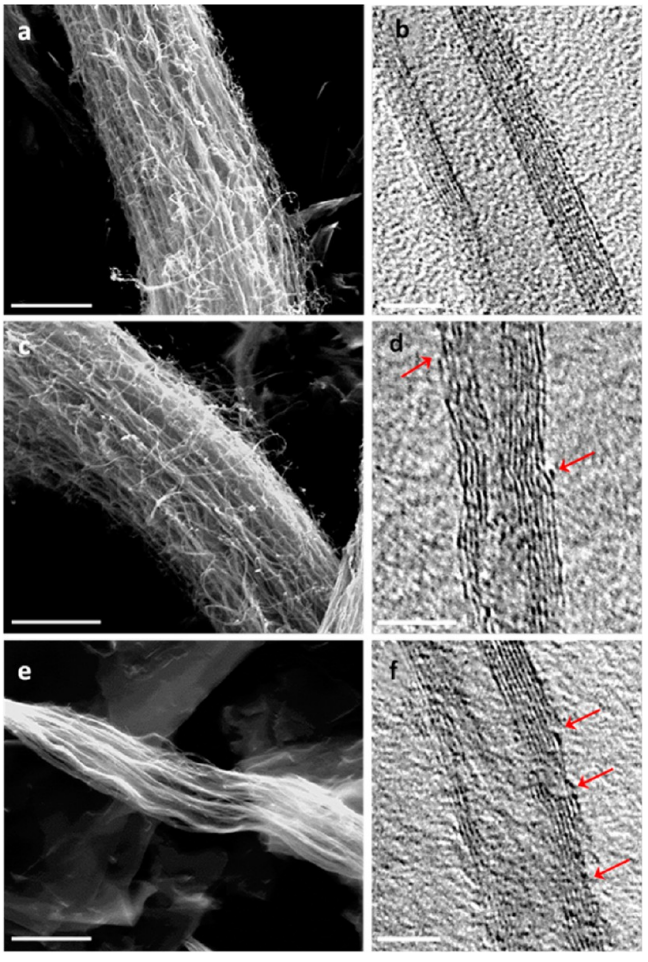

Figure 3. Representative SEM and TEM images of *k*-MWCNTs (a, b) as-received, (c, d) fluidized for 10 min, and (e, f) fluidized for 90 min. Scale bars represent 1 μm and 5 nm for SEM and TEM images, respectively. Red arrows demarcate sidewall functionalization.

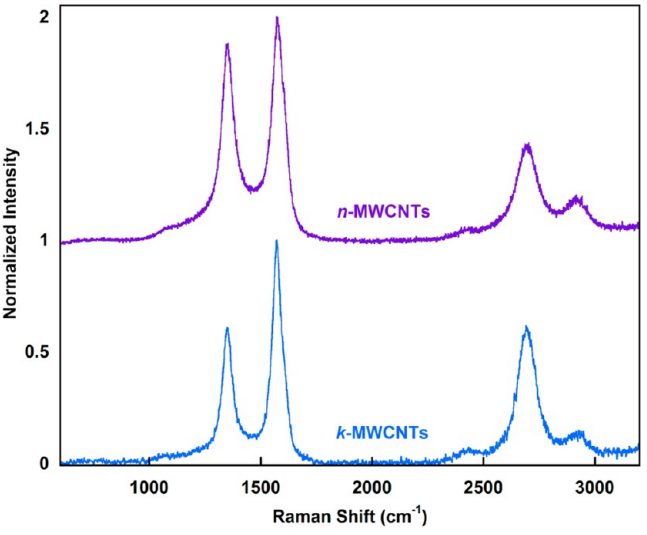

Figure 4. Representative Raman spectra of *n*-MWCNTs and *k*-MWCNTs.

significant differences in the bundling morphology of the *k*-MWCNTs and *n*-MWCNTs, structurally, the two types of nanotubes are dissimilar. Figure 2b reveals the presence of amorphous carbon on the surface of pristine *n*-MWCNTs that is absent from the pristine *k*-MWCNTs, as shown in Figure 3b.

Raman spectroscopy, a sensitive probe of CNT structure, also confirmed structural differences, as seen in the representative spectra of *k*-MWCNTs and *n*-MWNCTs given in Figure 4. Two prominent spectral features at 1354 and 1575 cm^{-1} correspond to a defect-induced disorder (D) peak and graphite (G) peak, respectively. The ratio of these peak areas, R = D/G, reflects the defect density present in the MWCNTs. Pristine *k*-MWCNTs had R = 0.66, whereas *n*-MWCNTs had R = 0.95, indicating that the *n*-MWCNTs contained many more sp^3-hybridized carbon atoms, which correspond to defect sites and amorphous carbon.

3.2. Effect of Oxidation on MWCNT Structure. The effects of ozone treatment on MWCNT structure were monitored with SEM. Representative images of *n*-MWCNT and *k*-MWCNT are given in Figures 2 and 3, respectively. No obvious shortening of the nanotubes was observed for either type of MWCNT. However, the average MWCNT bundle size decreased with increasing exposure, and this change in bundle morphology was manifested on the macroscopic scale by a transition from tightly packed spherical particles to low density, fluffy foams. MWCNT debundling is thought to occur from (i) physical separation by gas flow through the bundles during

dx.doi.org/10.1021/am4048305 | ACS Appl. Mater. Interfaces 2014, 6, 1835−1842

fluidization as well as (ii) chemical changes on the surface of the MWCNTs including removal of amorphous carbon between nanotubes and the introduction of functional groups on the nanotube sidewalls.

Structural changes were probed further with TEM. Comparison of Figure 2, panels b, d, and f reveals that amorphous carbon originally present on pristine *n*-MWCNTs is removed after 10 min of O_3 exposure and does not reappear upon further treatment up to 90 min. In addition, small breaks in the outer sidewalls of *n*-MWCNT exposed to O_3 are visible, whereas the inner walls remain intact. These features are indicative of oxidation originating at the MWCNT surface. Figure 3, panels b, d, and f also illustrates changes in *k*-MWCNT structure with increasing O_3 exposure. No amorphous carbon was visible in any *k*-MWCNTs, including the pristine samples. However, as with *n*-MWCNTs, imperfections in the outer walls of the nanotubes were observed after O_3 treatment. Notably, even after oxidation for 90 min, the overall structure of both types of tubes was largely intact, which is important for retention of mechanical properties.

3.3. FTIR Spectroscopy. The surface chemistry of pristine and treated MWCNTs was studied with the complementary techniques of FTIR spectroscopy, XPS, and Boehm titration. Figure 5 presents typical FTIR spectra of *n*-MWCNTs and *k*-MWCNTs normalized to the peak observed near 1580 cm^{-1} in all samples, which is attributed to infrared active vibration modes of the curved graphene lattices comprising the MWCNTs.[28] The broad peak centered at about 3445 cm^{-1} originates from −OH stretching of hydroxyl groups and ambient moisture adsorbed on the MWCNT surface. The weak bands at 2849 and 2918 cm^{-1} (C−H stretching) are ascribed to the presence of CH_2 moieties, which implies that the structures of both types of MWCNTs are more complex than simple sheets of rolled graphene. Similar observations have been reported previously for MWCNTs synthesized by CVD, with potentially significant implications for the oxidation mechanism when hydroxyl radicals are involved.[29] Interestingly, treatment of both types of MWCNTs causes the relative intensities of these peaks to increase significantly after 10 min of fluidization and subsequently decrease with further O_3 exposure. Comments on this behavior will be expanded upon later in this article when discussing XPS results. The sharp band observed at 1384 cm^{-1} is attributed to bending of −OH groups.[30] The low intensity of this peak in the case of pristine *n*-MWCNTs indicates that few hydroxyl groups are present in the as-received state. However, the relative intensity increases dramatically upon O_3 exposure for 10 min before decreasing with increased treatment time, meaning that significant numbers of hydroxyl groups are added to *n*-MWCNTs early in the reaction before they are subsequently depleted. Despite the lack of oxygenated defects found by XPS (vide infra), a peak at 1384 cm^{-1} is present in the spectrum of pristine *k*-MWCNTs. The intensity of this band increases upon O_3 treatment and remains a prevailing feature in the spectra of all functionalized samples. A band at about 1635 cm^{-1} corresponds to C═O stretching of quinone groups and another at 1735 cm^{-1} derives from COOH groups. Quinone groups are present in all MWCNTs. Although carboxylic acid moieties are present in pristine *n*-MWCNTs, after 10 min of exposure, the band at 1735 cm^{-1} nearly disappears, which could be due to complete oxidation of carboxylic acid-bearing amorphous carbon present on the nanotube surface. Pristine *k*-MWCNTs do not have a discernible peak at 1735 cm^{-1}, although O_3 exposure causes one to appear. The intensity of this peak is greatest for both types of MWCNTs after a long treatment time of 60 min. The concomitant increase in intensity of the carboxylic acid band and decrease in intensity of the hydroxyl peak with prolonged O_3 treatment could be the result of oxidation of the −OH groups to form COOH moieties.

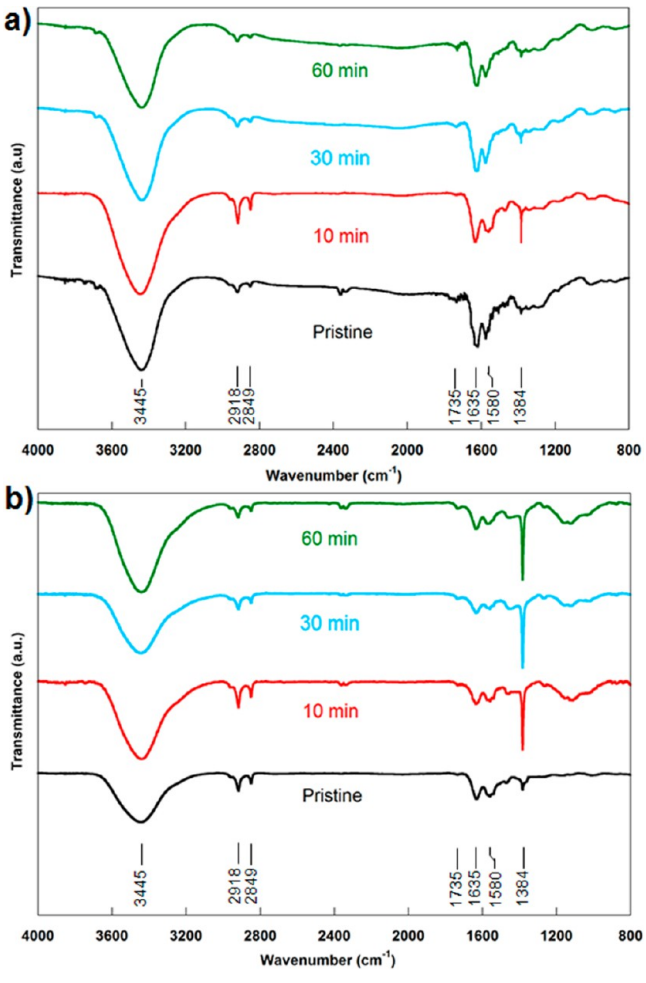

Figure 5. FTIR spectra of (a) *n*-MWCNTs and (b) *k*-MWCNTs.

3.4. XPS and Raman Analysis. While FTIR can help to elucidate the nature of functional groups grafted to the MWCNT, the technique is not amenable to quantitative analysis. To understand better the nature of changes in surface composition before and after oxidation, XPS was employed. Figure 6 shows representative survey spectra taken of *n*-MWCNTs and *k*-MWCNTs as a function of O_3 treatment time. The peaks centered at 532.0 eV, which correspond to O 1s photoelectrons, have been normalized to their respective C 1s peaks at 284.6 eV to allow direct comparison of their intensities across samples treated for different times. Clearly, the amount of oxygen increases with exposure time for both MWCNT varieties, although *n*-MWCNTs oxidize more gradually than *k*-MWCNTs with time. Quantitative analyses of the XPS spectra are summarized in Figure 7. As-received *n*-MWCNTs contain 2.3 atom % oxygen, whereas pristine *k*-MWCNTs have a negligible 0.5 atom %. Ten minutes of O_3 exposure increased the surface oxygen level to 4.2 atom % for *n*-

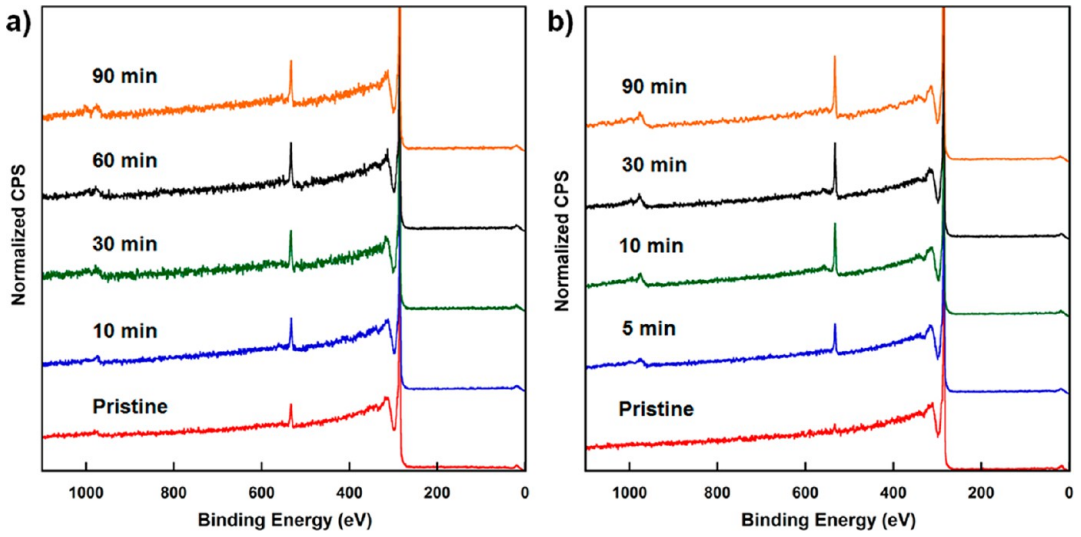

Figure 6. XPS survey spectra of (a) *n*-MWCNTs and (b) *k*-MWCNTs as a function of O_3 exposure time. All spectra are normalized to the C 1s peak.

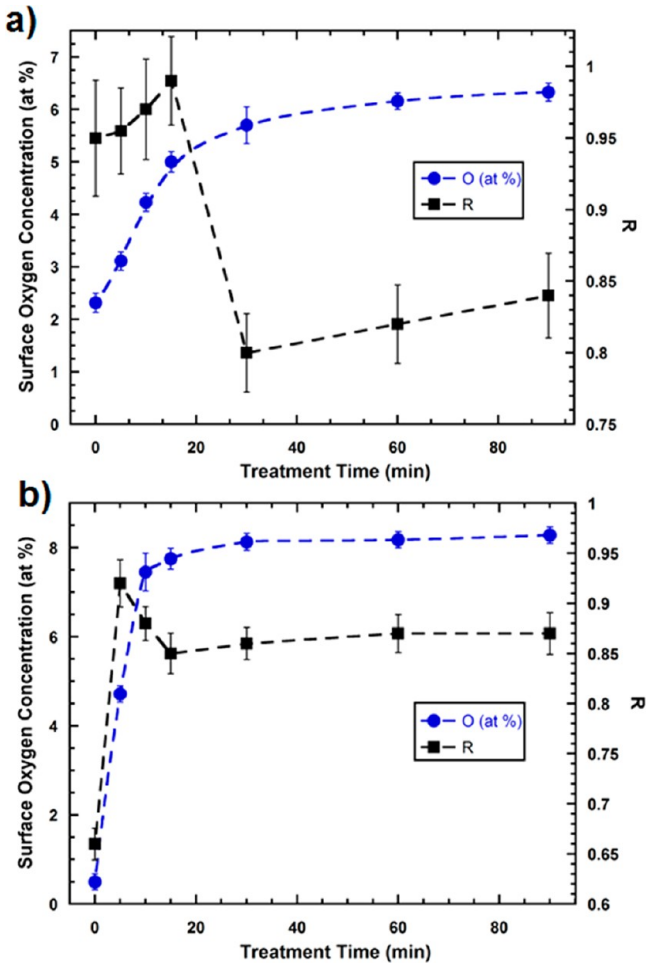

Figure 7. R values obtained from Raman spectra and surface oxygen concentration of (a) *n*-MWCNTs and (b) *k*-MWCNTs.

MWCNT and 7.5 atom % for *k*-MWCNT. After 90 min of fluidization, the amount of surface oxygen began to plateau around 6.3 and 8.1 atom % for *n*-MWCNTs and *k*-MWCNTs, respectively. Because of the small MWCNT diameters, even the surface specific XPS signal probes several nanotube walls, and it is possible that an atomic oxygen content of approximately 10% translates to a fully functionalized outer wall.[31]

The oxidation levels found in this study together with TEM observations indicate that oxidation occurs predominantly on the outer sidewalls of the MWCNTs. Although the oxidation behavior of the two varieties of MWCNTs is not identical, similar trends in R were observed with Raman spectroscopy, as seen in Figure 7. As both types of MWCNTs are oxidized, R initially increases, then it decreases, and finally levels off with prolonged treatment times. Possible reasons for the evolution of defects in this manner are discussed below in terms of three stages. In the first stage, oxidation is rapid as defect sites are oxidized to form predominantly −OH groups, which can be further oxidized to carboxylic acids. R increases because of the formation of large numbers of sp^3-hybridized functional groups, which are symmetry-breaking defects that significantly increase the Raman D-band intensity. In the second stage, many −OH groups are oxidized to form carboxylic acids, whereas carboxylic acid groups formed previously on reactive amorphous carbon or adsorbed carbonaceous debris are further oxidized to CO_2. The loss of some oxidized species causes the apparent rate of oxidation to slow, although it still increases because of the introduction of large amounts of oxygen in the form of carboxylic acid groups. R decreases slightly at this stage as defects are completely oxidized away. At a certain point, the reactive carbon defects present initially are completely oxidized, and the majority of −OH groups on the nanotube surfaces have oxidized to form carboxylic acids. At this final stage, the number of carboxylic acid groups formed and completely oxidized stabilizes, and both R and the surface oxygen concentrations do not vary appreciably with additional exposure time.

Figure 7 illustrates that although the overall trends involving changes in R and O atom % with exposure time are similar for both types of MWCNTs, they differ in time scales and magnitude. This is likely due to differences in the initial defect structures of the two MWCNT varieties. *n*-MWCNTs contain a significant number of defects in the as-received state (R = 0.95), whereas pristine *k*-MWCNTs possess relatively low defect densities (R = 0.66). Initial oxidation causes little change in the R value of *n*-MWCNTs, as the complete oxidation of amorphous carbon may balance out the contributions of

dx.doi.org/10.1021/am4048305 | ACS Appl. Mater. Interfaces 2014, 6, 1835−1842

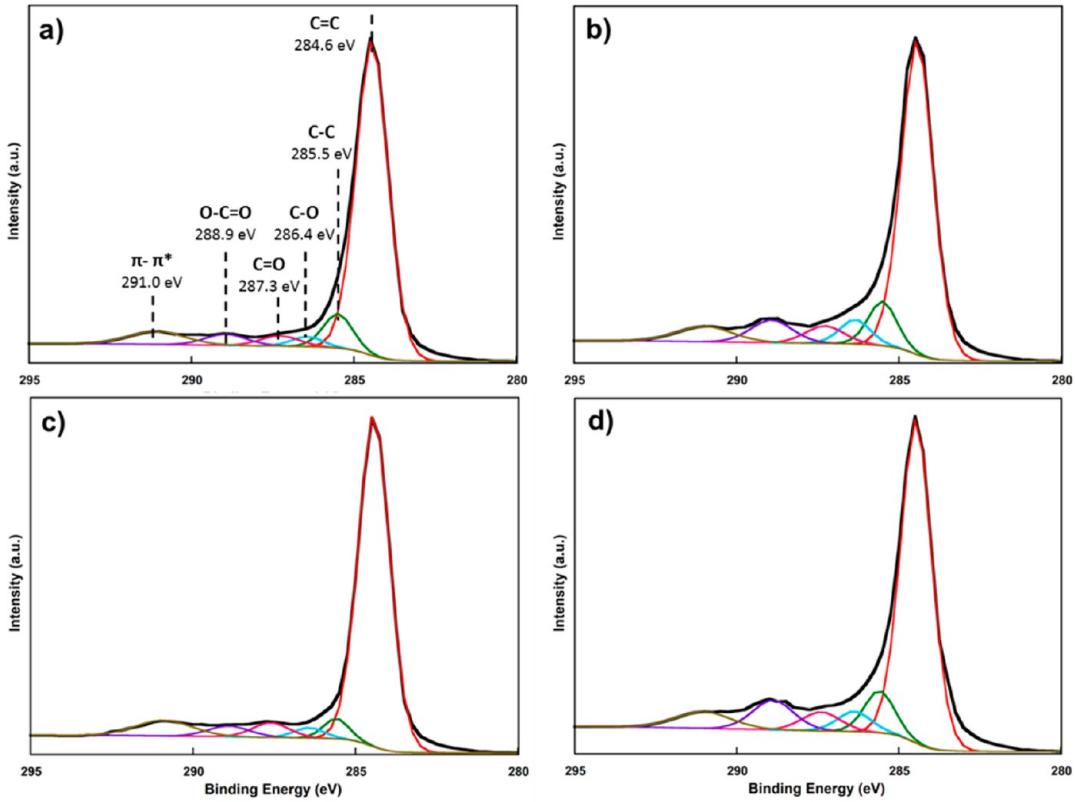

Figure 8. High-resolution XPS C 1s spectra of (a) pristine and (b) 90 min O_3 *n*-MWCNTs as well as (c) pristine and (d) 90 min O_3 *k*-MWCNTs.

nanotube sidewall oxidation on the Raman D-band intensity. In contrast, R increases rapidly to 0.88 after 10 min of O_3 exposure for *k*-MWCNTs as large numbers of symmetry-breaking functional groups are introduced on the nanotube surfaces without amorphous carbon removal. The differences in the apparent oxidation rate of *n*-MWCNTs and *k*-MWCNTs observed by XPS are believed to be directly linked to their dissimilarities in initial defect densities. However, despite initial differences in defect structure, *k*-MWCNTs and *n*-MWCNTs treated for at least 30 min with O_3 have similar R values at similar levels of oxidation. This trend indicates that after removal of amorphous carbon, the Raman D band stems primarily from sidewall functionalization and that defects initially present in *n*-MWCNTs are completely removed during the early stages of oxidation. It should be noted that defects can also arise from mechanical ablation of the MWCNTs. To ensure that fluidization has no effect on the nanotube structure, a control experiment was performed using compressed air in place of O_3 as the bubbling gas. No changes in R were observed for pristine *n*-MWCNTs or *k*-MWCNTs after 90 min of treatment, indicating that the fluidization forces are not sufficient to mechanically damage the nanotubes.

XPS is very sensitive to the bonding environment of carbon atoms, and high-resolution scans of the C 1s envelope can be used to identify and compare the number of functional groups present on the surface of a MWCNT. Figure 8 shows representative high-resolution C 1s spectra of the pristine and treated MWCNTs, which have been fitted with six peaks. The peaks correspond to graphitic sp^2-hybridized carbon (284.6 eV), sp^3-hybridized defects including hydrocarbons (285.5 eV), hydroxyl or ether groups (286.4 eV), carbonyl groups (287.3 eV), carboxylic or ester groups (288.9 eV), and $\pi-\pi^*$ "shakeup" transitions (291.0 eV).[32]

The relative distribution of oxygen-bearing functional groups present on the surface of *n*-MWCNTs as a function of treatment time is summarized in Figure 9a. The fraction of C−O groups increased rapidly during the first 10 min of exposure and then decreased slightly upon further treatment. In contrast, the fractions of C═O and O−C═O moieties did not increase until exposure times greater than 30 min, suggesting that C−O groups are oxidized to become C═O and O−C═O groups. The large fraction of sp^3-hybridized carbon initially present in *n*-MWCNTs reflects the structural disorder in as-received nanotubes. After 30 min of oxidation, the relative number of C−C bonds decreases slightly before increasing upon further oxidation. Figure 9b summarizes the functional group evolution with treatment time for *k*-MWCNTs. The fraction of C−C and O−C═O groups increase more quickly for *k*-MWCNTs than for *n*-MWCNTs, whereas the rate of C−O generation is similar. As with *n*-MWCNTs, the number of C═O moieties increases slightly throughout the reaction. Unlike *n*-MWCNTs, which contain some amorphous carbon on the surface, pristine *k*-MWCNTs possess relatively few C−C bonds. However, upon exposure to O_3, *k*-MWCNTs quickly develop a large fraction of sp^3-hybridized carbon bonds up to about 8%. This C−C fraction is similar to that of *n*-MWCNTs oxidized to the same degree and suggests that in the case of *n*-MWCNTs the relatively steady percentage of C−C bonds observed with oxidation time is due to a balance between the complete oxidation of sp^3 defects initially present in the form of amorphous carbon and the formation of sp^3 defects in the nanotube sidewall through covalent functionalization. This idea is further supported by the evolution of the $\pi-\pi^*$ peak, which is sensitive to the aromatic character of the nanotubes. In the case of *n*-MWCNTs, the $\pi-\pi^*$ intensity increases initially before deceasing after 15 min of O_3 exposure, suggesting that

dx.doi.org/10.1021/am4048305 | ACS Appl. Mater. Interfaces 2014, 6, 1835−1842

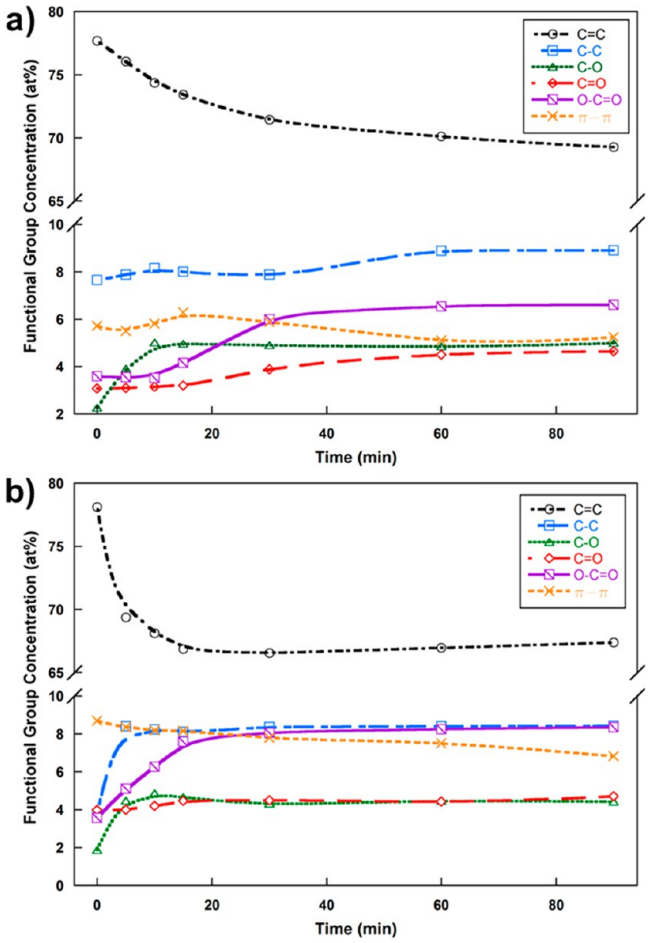

Figure 9. Relative functional group concentrations obtained from deconvolution of high-resolution XPS scans for (a) *n*-MWCNTs and (b) *k*-MWCNTs as a function of treatment time.

amorphous carbon is removed to reveal the graphitic nanotube walls followed by sidewall functionalization. The intensity of the $\pi-\pi^*$ peak simply decreases with treatment time for *k*-MWCNTs as the sidewall is oxidized immediately in the absence of amorphous carbon.

3.5. Titration. To complement surface functional group analysis by photoelectron spectroscopy, the amounts of acidic functionalities present on the surface of the MWCNTs were analyzed with chemical titration following the method of Boehm. Figure 10a summarizes the results of titrating *n*-MWCNTs subjected to different O_3 treatment times. The results agree well with XPS in that the formation of −OH groups is favored for short reactions times, whereas carboxylic acids are generated after long exposure times. A similar trend is observed for *k*-MWCNTs except that a greater number of lactonic species are formed early in the reaction, as shown in Figure 10b. As with FTIR and XPS analyses, these results suggest that hydroxyl groups formed at short exposure times may act as an intermediate species that is further oxidized into carbonyl and carboxylic acid groups upon further exposure.

3.6. Homogeneity of Oxidation. To be suitable for industrial use, MWCNT-functionalization reactions must produce relatively homogeneous oxidation levels throughout large sample volumes. This is a challenge for any gas-phase reaction, and previous work has shown that gaseous O_3 oxidation of CNTs is particularly difficult because oxidation is restricted to the outer surface of a CNT conglomerate.[19] This section will compare the variance in the oxidation levels achieved in the present study with those previously reported for both traditional liquid-phase acid treatments and other gas-phase routes. Here, we define homogeneity as the uniform composition of small volumes of nanotubes within a larger volume subjected to the same treatment.

Despite extensive published research, literature reports of oxidation variance within a given experiment are scarce. This may be due to the fact that, to date, most oxidation is done in solution with acids and the scatter is relatively small. The few reported error ranges for acid-oxidized CNTs seem to support this assertion. Using nitric acid to oxidize MWCNTs, Andrade and co-workers found only a 2.9% relative standard deviation of the mean oxidation level of 3.5 atom %, as determined by EDS.[33] Although each EDS measurement probes a relatively large volume of nanotubes, the consistency of the results across the samples suggests that the nanotubes were homogeneously oxidized. Similarly, Wang et al. reported relative standard deviations on the order of 1−9% for triplicate titration measurements of the acidic functional groups present in

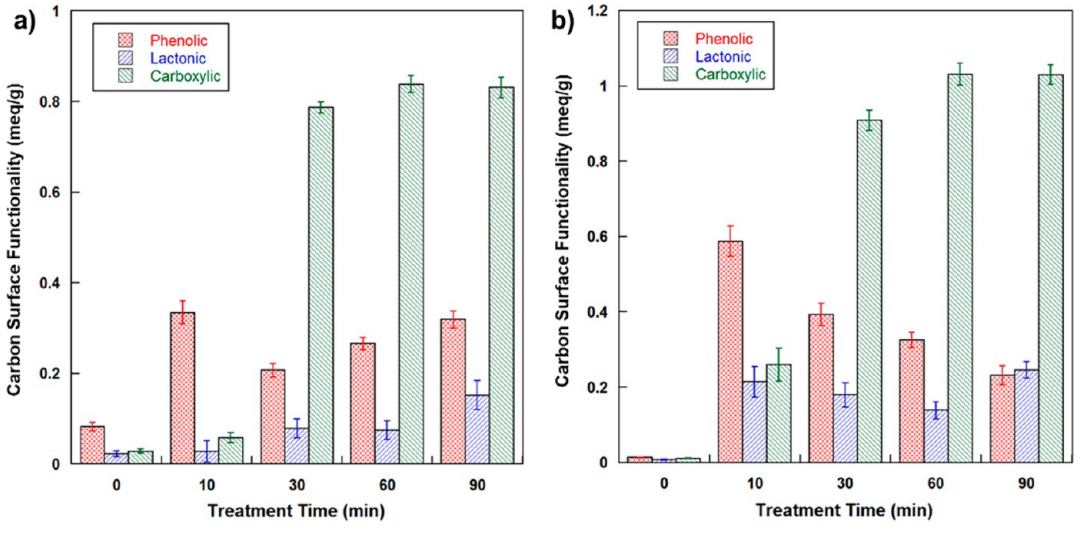

Figure 10. Protic functional group concentrations obtained from Boehm titration of (a) *n*-MWCNTs and (b) *k*-MWCNTs.

dx.doi.org/10.1021/am4048305 | ACS Appl. Mater. Interfaces 2014, 6, 1835−1842

MWCNTs that had been refluxed in nitric acid and washed with NaOH.[34]

In contrast, gas-phase reactions tend to be much less homogeneous. Byl and co-workers found that O_3 oxidation of SWCNTs is highly dependent on their geometrical surface area but nearly independent of specific surface area.[19] Upon exposure to gaseous O_3, only SWCNTs on the outermost geometric surface of the nanotube agglomerate were oxidized. An early attempt to thermally oxidize MWCNTs in air also resulted in a broad distribution of oxidation levels. Ajayan and co-workers reported a relative standard deviation of 49% for thermogravimetric measurements of the nanotubes after 9.9 wt % loss to oxidation at 700 °C.[35] They attributed this large variation partially to differences in the availability of oxygen to samples with different geometric surface areas.

In this study, XPS and Boehm titration were used to characterize the extent of oxidation through measurements of many small aliquots of MWCNTs taken from the larger oxidized volume. Although XPS is a surface sensitive technique, it has limited spatial resolution, so each measurement probes many MWCNTs at once. Therefore, both titration and XPS results give a measure of the bulk functionalization homogeneity but not necessarily the uniformity of oxidation along any given nanotube. The XPS and titration measurements performed in this study have relative standard deviations in the range of 2−5% and 1−12%, respectively, for samples with appreciable levels of oxidation. These figures are similar to those reported for liquid-phase acid reactions and suggest that fluidization of the MWCNTs in O_3 produces relatively homogeneous levels of oxidation.[36,37]

4. CONCLUSIONS

Fluidizing MWCNTs in gas-phase O_3 proved effective at uniformly functionalizing the MWCNT sidewalls without destroying the nanotube structure and without the use of any solvents or additional purification steps. Comparison of two nominally similar MWCNTs with different defect structures revealed that this treatment can also purify MWCNTs from amorphous carbon in short periods of time. We suggest that this defect removal causes the apparent oxidation rate of *n*-MWCNTs to be lower than *k*-MWCNTs. Characterization of oxidized MWCNTs revealed that oxidation proceeds through the formation of predominantly −OH groups initially, which become further oxidized to C═O and COOH groups upon greater O_3 exposure. Although the exact mechanism of oxidation was not determined, the presence of aliphatic defects seems to play a significant role. Because the fluidized O_3 reaction reported herein is solvent-free, simple, and does not destroy the nanotube structure, we believe it offers an attractive route for functionalizing MWCNTs on an industrial scale.

AUTHOR INFORMATION

Corresponding Author

*E-mail: michaelr.kessler@wsu.edu.

Notes

The authors declare no competing financial interest.

REFERENCES

(1) Im, J. S.; Chang Kang, S.; Bai, B. C.; Suh, J.-K.; Lee, Y.-S. *Int. J. Hydrogen Energy* **2011**, *36*, 1560−1567.
(2) Oriňáková, R.; Oriňák, A. *Fuel* **2011**, *90*, 3123−3140.
(3) Wang, C.; Takei, K.; Takahashi, T.; Javey, A. *Chem. Soc. Rev.* **2013**, *42*, 2592−2609.
(4) So, H.-M.; Won, K.; Kim, Y. H.; Kim, B.-K.; Ryu, B. H.; Na, P. S.; Kim, H.; Lee, J.-O. *J. Am. Chem. Soc.* **2005**, *127*, 11906−11907.
(5) Han, C.; Doepke, A.; Cho, W.; Likodimos, V.; de la Cruz, A. A.; Back, T.; Heineman, W. R.; Halsall, H. B.; Shanov, V. N.; Schulz, M. J.; Falaras, P.; Dionysiou, D. D. *Adv. Funct. Mater.* **2012**, *23*, 1807−1816.
(6) Lau, K.-T.; Shi, S.-Q.; Zhou, L.-M.; Cheng, H.-M. *J. Compos. Mater.* **2003**, *37*, 365−376.
(7) Guadagno, L.; De Vivo, B.; Di Bartolomeo, A.; Lamberti, P.; Sorrentino, A.; Tucci, V.; Vertuccio, L.; Vittoria, V. *Carbon* **2011**, *49*, 1919−1930.
(8) Zhu, J.; Peng, H.; Rodriguez-Macias, F.; Margrave, J. L.; Khabashesku, V. N.; Imam, A. M.; Lozano, K.; Barrera, E. V. *Adv. Funct. Mater.* **2004**, *14*, 643−648.
(9) Zhu, J.; Kim, J.; Peng, H.; Margrave, J. L.; Khabashesku, V. N.; Barrera, E. V. *Nano Lett.* **2003**, *3*, 1107−1113.
(10) Yuen, S.-M.; Ma, C.-C. M.; Lin, Y.-Y.; Kuan, H.-C. *Compos. Sci. Technol.* **2007**, *67*, 2564−2573.
(11) Kim, J. Y.; Han, S. I.; Hong, S. *Polymer* **2008**, *49*, 3335−3345.
(12) Eitan, A.; Jiang, K.; Dukes, D.; Andrews, R.; Schadler, L. S. *Chem. Mater.* **2003**, *15*, 3198−3201.
(13) Verdejo, R.; Lamoriniere, S.; Cottam, B.; Bismarck, A.; Shaffer, M. *Chem. Commun.* **2007**, *0*, 513−515.
(14) Shenderova, O.; Koscheev, A.; Zaripov, N.; Petrov, I.; Skryabin, Y.; Detkov, P.; Turner, S.; Van Tendeloo, G. *J. Phys. Chem. C* **2011**, *115*, 9827−9837.
(15) Mawhinney, D. B.; Naumenko, V.; Kuznetsova, A.; Yates, J. T.; Liu, J.; Smalley, R. E. *J. Am. Chem. Soc.* **2000**, *122*, 2383−2384.
(16) Cai, L.; Bahr, J. L.; Yao, Y.; Tour, J. M. *Chem. Mater.* **2002**, *14*, 4235−4241.
(17) Chen, Z.; Ziegler, K. J.; Shaver, J.; Hauge, R. H.; Smalley, R. E. *J. Phys. Chem. B* **2006**, *110*, 11624−11627.
(18) Lu, X.; Zhang, L.; Xu, X.; Wang, N.; Zhang, Q. *J. Phys. Chem. B* **2002**, *106*, 2136−2139.
(19) Byl, O.; Liu, J.; Yates, J. T. *Langmuir* **2005**, *21*, 4200−4204.
(20) Liu, Z.-Q.; Ma, J.; Cui, Y.-H.; Zhang, B.-P. *Appl. Catal., B* **2009**, *92*, 301−306.
(21) Morales-Lara, F.; Pérez-Mendoza, M. J.; Altmajer-Vaz, D.; García-Román, M.; Melguizo, M.; López-Garzón, F. J.; Domingo-García, M. *J. Phys. Chem. C* **2013**, *117*, 11647−11655.
(22) Wepasnick, K. A.; Smith, B. A.; Schrote, K. E.; Wilson, H. K.; Diegelmann, S. R.; Fairbrother, D. H. *Carbon* **2011**, *49*, 24−36.
(23) Sham, M.-L.; Kim, J.-K. *Carbon* **2006**, *44*, 768−777.
(24) Cataldo, F. *Fullerenes, Nanotubes, Carbon Nanostruct.* **2008**, *16*, 1−17.
(25) Peng, K.; Liu, L.-Q.; Li, H.; Meyer, H.; Zhang, Z. *Carbon* **2011**, *49*, 70−76.
(26) Kuyate, P. S.; Patel, V. *Nanotech Insights* **2011**, 39−44.
(27) Goertzen, S. L.; Thériault, K. D.; Oickle, A. M.; Tarasuk, A. C.; Andreas, H. A. *Carbon* **2010**, *48*, 1252−1261.
(28) Jishi, R. A.; Venkataraman, L.; Dresselhaus, M. S.; Dresselhaus, G. *Chem. Phys. Lett.* **1993**, *209*, 77−82.
(29) Li, W.; Bai, Y.; Zhang, Y.; Sun, M.; Cheng, R.; Xu, X.; Chen, Y.; Mo, Y. *Synth. Met.* **2005**, *155*, 509−515.
(30) Ma, P. C.; Kim, J.-K.; Tang, B. Z. *Carbon* **2006**, *44*, 3232−3238.
(31) Haiber, S.; Ai, X.; Bubert, H.; Heintze, M.; Brüser, V.; Brandl, W.; Marginean, G. *Anal. Bioanal. Chem.* **2003**, *375*, 875−883.
(32) Simmons, J. M.; Nichols, B. M.; Baker, S. E.; Marcus, M. S.; Castellini, O. M.; Lee, C. S.; Hamers, R. J.; Eriksson, M. A. *J. Phys. Chem. B* **2006**, *110*, 7113−7118.
(33) Andrade, N.; Martinez, D.; Paula, A.; Silveira, J.; Alves, O.; Souza Filho, A. *J. Nanopart. Res.* **2013**, *15*, 1−11.
(34) Wang, Z.; Shirley, M. D.; Meikle, S. T.; Whitby, R. L. D.; Mikhalovsky, S. V. *Carbon* **2009**, *47*, 73−79.
(35) Ajayan, P. M.; Ebbesen, T. W.; Ichihashi, T.; Iijima, S.; Tanigaki, K.; Hiura, H. *Nature* **1993**, *362*, 522−525.
(36) Banerjee, S.; Wong, S. S. *J. Phys. Chem. B* **2002**, *106*, 12144−12151.
(37) Li, M.; Boggs, M.; Beebe, T. P.; Huang, C. P. *Carbon* **2008**, *46*, 466−475.